Static density response function studied by inelastic x-ray scattering: Friedel oscillations in solid and liquid Li

Toru Hagiya,[1,*] Kazuhiro Matsuda,[1,†] Nozomu Hiraoka,[2] Yukio Kajihara,[3] Koji Kimura,[4] and Masanori Inui[3]

[1]*Graduate School of Science, Kyoto University, Kyoto 606-8502, Japan*

[2]*National Synchrotron Radiation Research Center, Hsinchu 30076, Taiwan*

[3]*School of Integrated Arts and Sciences, Hiroshima University, Higashi Hiroshima 739-8521, Japan*

[4]*Department of Physical Science and Engineering, Nagoya Institute of Technology, Nagoya 466-8555, Japan*

(Received 11 October 2019; revised 10 July 2020; accepted 5 August 2020; published 21 August 2020)

We performed inelastic x-ray scattering experiments on solid and liquid Li to determine the static density response function $\chi(q, 0)$, where q is wave vector. The experimentally determined $\chi(q, 0)$ allows meaningful comparison of the response function with that of the electron gas model; $\chi(q, 0)$ exhibits the $2k_F$ singularity predicted in the electron gas model. The screening electron density induced by a positive point charge is calculated, and it shows Friedel oscillations both in solid and liquid Li. Moreover, we found that the Friedel oscillations become weak upon melting.

DOI: 10.1103/PhysRevB.102.054208

I. INTRODUCTION

Screening is an important concept for describing the effective interaction in electron gas, because the bare Coulomb interaction is modified by screening electrons. According to the linear response theory, the static screening electron density induced by external potential is expressed by the static density response function $\chi(\mathbf{q}, \omega = 0)$ as $\Delta n(\mathbf{q}) = V_{\text{ext}}(\mathbf{q})\chi(\mathbf{q}, \omega = 0)$ [1]; $\hbar\mathbf{q}$ and $\hbar\omega$ are the momentum and energy transfer, respectively. A typical example of the density response function is that of the random-phase approximation (RPA), and it shows a singularity at $|\mathbf{q}| = 2k_F$ [1,2]. This singularity is the origin of Friedel oscillations in the screening electron density [3]. The many-body effects beyond the RPA on screening can be treated with the local field correction $G(q)$ [1]. Enormous theoretical effort toward the construction of $G(q)$ has been made, aiming at a deeper understanding of the screening [1,4,5].

There have been a number of experimental studies on investigating physical quantities that reflect screening in metals. The standing waves related to Friedel oscillations can be observed by scanning tunneling microscopy [6,7], and their measurements have been performed recently for various metallic surfaces [8–11]. In principle, the measured standing waves allowed the reconstruction of the screening electron density [12,13], but the reconstruction by scanning tunneling microscopy experiments has not been accomplished to our knowledge. In the field of liquid metals, the effective interionic potential, screened by valence electrons, was determined from the experimentally obtained liquid structure factor [14]. It is well known that the experimentally determined effective interionic potential shows the $2k_F$ oscillation in liquid states [15]. Although it is possible to obtain indirect information on screening through the effective interionic potential, this approach does not provide $\chi(\mathbf{q}, 0)$, which is a key quantity for describing screening.

Recently, the development of inelastic x-ray scattering (IXS) techniques has enabled the determination of the density response function of electrons [16,17]. In IXS experiments, the double-differential cross section is related to the dynamic structure factor $S(\mathbf{q}, \omega)$:

$$\frac{d^2\sigma}{d\Omega d\omega} = \left(\frac{d^2\sigma}{d\Omega d\omega}\right)_{\text{Th}} S(\mathbf{q}, \omega), \tag{1}$$

where $(d^2\sigma/d\Omega d\omega)_{\text{Th}}$ is the Thompson scattering cross section [18]. The imaginary part of the density response function can be calculated on the basis of the fluctuation dissipation theorem by $\text{Im}[\chi(\mathbf{q}, \omega)] = -\pi S(\mathbf{q}, \omega)$. Although the IXS experiments provide only the imaginary part, the real part can be reconstructed by the Kramers–Kronig (K–K) transformation. With this procedure, Abbamonte and coworkers determined the density response function and discussed the attosecond electron dynamics in condensed matter [16,17]. In addition to the electron dynamics, importantly, information on *static* screening can be deduced from the *dynamic* structure factor. Reed *et al.* determined $\chi(\mathbf{q}, \omega = 0)$ by the K–K transformation of $\text{Im}[\chi(\mathbf{q}, \omega)]$. They calculated the screening electron density of graphene by using $\chi(\mathbf{q}, 0)$ and showed that the charge impurity is screened nearly completely in a few nanometers [19].

In this study, we carried out IXS experiments on solid and liquid Li to determine $\chi(\mathbf{q}, 0)$. Li is suited for investigating screening in simple metals for the following reasons. (i) The valence electron of Li is well described with the electron gas model. (ii) It is possible to obtain strong IXS signals

[*]Present address: Metal Powder Technology Department, Sanyo Special Steel Co., Ltd., Himeji, Hyogo 672-8677, Japan.

[†]Present address: Department of Physics, Kumamoto University, Kumamoto 860-8555, Japan.

because of the small x-ray attenuation. (iii) Extensive knowledge regarding $S(\mathbf{q}, \omega)$ of Li has been accumulated [20–25]. Furthermore, we compared the results for the solid and the liquid to reveal the effect of disorder on the $2k_F$ singularity. In liquid states, the Fermi surface is blurred owing to the effect of disorder [15,26,27]. Although the effect of Fermi surface blurring on screening has been theoretically investigated [28–30], experimental information on this effect is sparse.

We have determined $\chi(\mathbf{q}, 0)$ of solid and liquid Li with IXS measurements over a wide range of momentum and energy transfer. The experimentally obtained $\chi(\mathbf{q}, 0)$ enables meaningful comparison of the response function with that of the electron gas model. The screening electron density is calculated using $\chi(\mathbf{q}, 0)$, and the calculated density exhibits Friedel oscillations. We find that the amplitude of the Friedel oscillations in the liquid tends to be smaller than in the solid because of the scattering effects of disordered ions.

II. EXPERIMENT

We carried out the IXS measurements at the Taiwan IXS beamline BL12XU at SPring-8. The synchrotron radiation from the undulator light source was first monochromatized with a cryogenic Si (111) double crystal and then a pair of Si (220) channel-cut crystals. The incident photon energy E_0 was fixed at 19.98 keV. In order to obtain inelastic spectra, the scattered photons were reflected by a Si (660) triangular crystal before being counted by an NaI scintillation detector [31]. The scattered photon energy E was scanned from -10 eV to 350 eV in $E_0 - E = \hbar\omega$ [32]. The range of the energy scan was very wide compared with that in usual IXS experiments [20–25] so that the K–K transformation could be performed accurately. The energy resolution varied within 1.2–1.4 eV, depending on the scattering angle.

The IXS measurements were carried out for polycrystalline Li (RT) and liquid Li (493 K). The polycrystalline sample, whose crystal orientations is averaged, was used in order to compare best the spectra with the liquid. Thus, we denote the dynamic structure factor as $S(q, \omega)$, with $q = |\mathbf{q}|$. The sample, which was contained in a metal cell made of molybdenum, was sealed in a chamber filled with He gas to avoid oxidation of the sample. The sample cell was heated with an Fe-Cr electronic resistant heater, and the temperature was monitored with alumel-chromel thermocouples. We collected 19 spectra in the range of 0.30–3.47 Å^{-1}. The maximum scattering angle was limited at 20° by the sample environment. For such a case, high energy x-rays are better because the wider q range is accessible. We chose 20 keV, which is significantly higher than usual energies. Another advantage of the 20 keV spectrometer is a large space around the sample chamber, because the detector positions are in the opposite side to the sample.

Elastic scattering was fitted by Voigt function and subtracted from the spectra. The subtracted spectra $I(q, \omega)$ were extrapolated, so that $I(q, \omega) = 0$ at $\hbar\omega = 0$, using Mermin's function [33]. $I(q, \omega)$ can be normalized with the valence electron density n by using the f-sum rule [18],

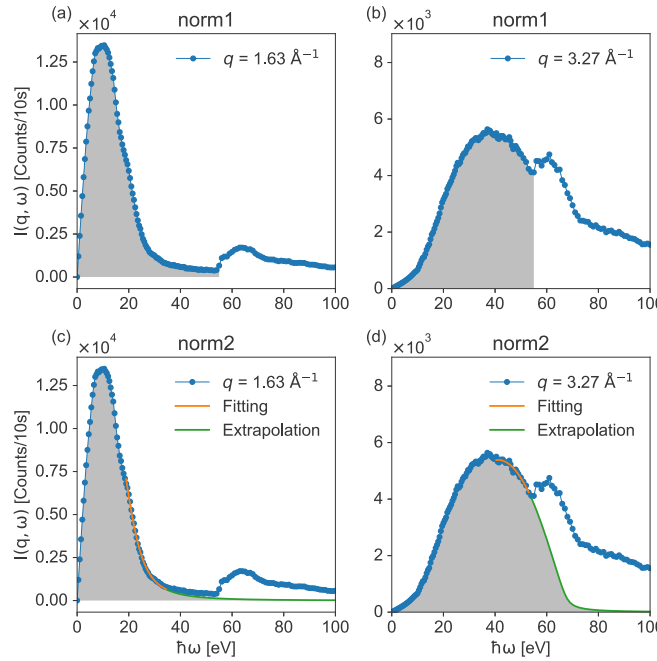

FIG. 1. (a), (b) Experimentally obtained IXS spectrum at $q = 1.63$ Å^{-1} and $q = 3.27$ Å^{-1}. The shaded area indicates the contribution of the f-sum integration calculated with the norm 1. (c), (d) Spectra at $q = 1.63$ Å^{-1} and $q = 3.27$ Å^{-1}. The fitting and extrapolated curve of norm 2 are plotted.

where the electron density of Li is $n_{\mathrm{sol}} = 0.046$ Å^{-3} and $n_{\mathrm{liq}} = 0.044$ Å^{-3}:

$$\int_0^\infty d\omega S(q, \omega)\omega = \frac{nq^2}{2m}. \tag{2}$$

However, the integration over the whole range did not provide an accurate absolute scale, because the IXS spectra in the energy range higher than 55 eV included the contribution of core electron excitations, as seen from Figs. 1(a) and 1(b). We applied two methods to determine the absolute scale from the valence contribution. In the first normalization method (norm 1), we terminated the f-sum integration at 55 eV, which can be seen from the shaded area in Figs. 1(a) and 1(b). In Fig. 1(b), the valence contribution also arises at higher energies than 55 eV, and the sum integrals cannot be properly evaluated in this q range. Thus, we determined a single normalization constant $C_1 = S(q, \omega)/I(q, \omega)$ from the sum integrals in $q < 1.63$ Å^{-1} and normalized all spectra with C_1 [34]. In the second method (norm 2), we extrapolated the valence contribution with Mermin's function [35]. Figures 1(c) and 1(d) show the extrapolated curve and the integrated region. We determined q-dependent normalization constants $C_2(q)$ from the integral of each extrapolated spectrum. These normalization methods have a small effect on the q dependence of the obtained $\chi(q, 0)$, however, the absolute scale of $\chi(q, 0)$ and the r dependence of the screening electron density depend on the choice of the normalization methods.

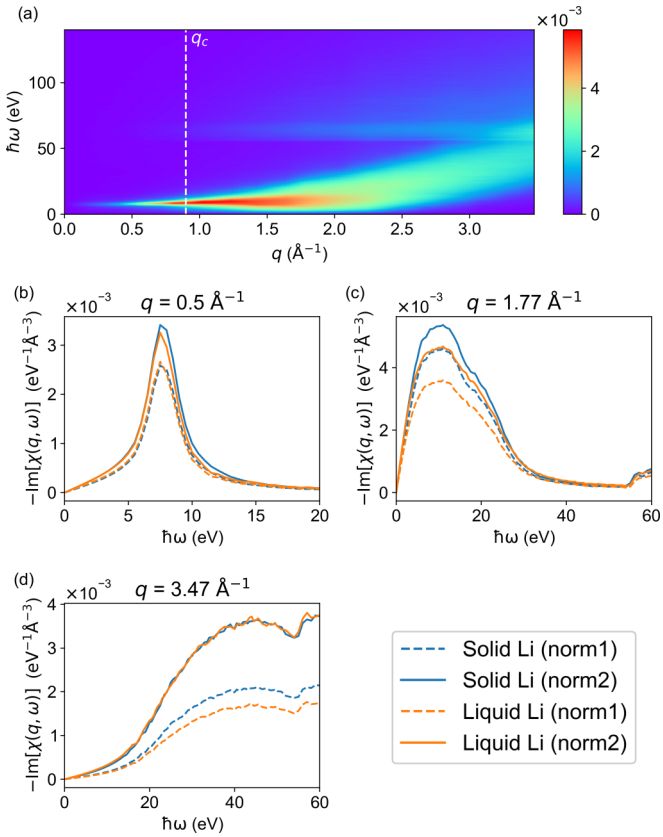

FIG. 2. (a) Experimentally determined $-\mathrm{Im}[\chi(q,\omega)]$ for solid Li. q_c is estimated to be 0.9 Å^{-1} using the electron gas model [36]. (b) $-\mathrm{Im}[\chi(q,\omega)]$ of solid and liquid Li at $q = 0.5$ Å^{-1}. The dashed and solid lines indicate the results obtained with the method of norm 1 and norm 2, respectively. (c) $-\mathrm{Im}[\chi(q,\omega)]$ at $q = 1.77$ Å^{-1}. (d) $-\mathrm{Im}[\chi(q,\omega)]$ at $q = 3.47$ Å^{-1}.

III. RESULTS AND DISCUSSION

A. IXS spectra

Figure 2(a) shows the IXS spectra for solid Li. In the low q range ($q < q_c$), a sharp peak of a plasmon is observed. q_c is the plasmon cutoff wave vector, beyond which the plasmon is strongly damped [36]. The plasmon energy and line width are presented in the Supplemental Material [34]. In the high q range ($q > q_c$), the excitation spectra are dominated by a broad feature consisting of single-particle excitations. In addition to the valence contribution, the K-edge structure is observed at around 55 eV, and the intensity of the K-edge structure increases with q.

The plasmon spectra of the solid and the liquid are compared in Fig. 2(b). The different normalization methods are indicated by solid and dashed lines. The shape of the plasmon excitation spectrum shows little change on melting. Figure 2(c) shows the spectra in the single-particle continuum for the solid and the liquid. The IXS spectrum for the solid shows a fine structure at around 17 eV. According to previous IXS measurements of solid Li [24], additional intensities due to the band structure effect appear, which results in the fine structure in the single-particle excitation spectrum. In the liquid state, the dip at around 17 eV is smeared, and no fine structure is observed. This is attributed to the reduction of the band structure effect upon melting, because in the liquid state the IXS intensity due to the band structure effect is expected to be small. Moreover, we note that the peak intensity of the IXS spectrum for the liquid is smaller than that for the solid, which should also reflect the reduction of the band structure effect. These trends upon melting are also observed for the spectra in $1.63 < q < 2.45$ Å^{-1} ($1.5 < q < 2.2\ k_F$), which are presented in the Supplemental Material [34]. In the higher q range [Fig. 2(d)], the spectra of the solid and liquid have similar shapes.

The absolute scale of $-\mathrm{Im}[\chi(q,\omega)]$ is affected by the normalization methods. In fact, the IXS intensity of the liquid gradually decreases with increasing q during a long measurement [34], which leads to a small value of $-\mathrm{Im}[\chi(q,\omega)]$ of norm 1 in the high q region. Such disadvantage of norm 1 can be compensated by the method of norm 2. In the case of norm 2, the normalization was carried out for each spectrum, and the problem of the variation of the IXS intensity was avoided. The method of norm 1 is a crude procedure, however, the results of norm 1 are useful to estimate how large uncertainty is caused by the extrapolation.

B. Static density response function

We calculate $\chi(q,0)$ using the K–K relation:

$$\mathrm{Re}[\chi(q,\omega)] = \frac{1}{\pi} P \int_{-\infty}^{\infty} d\omega' \frac{\mathrm{Im}[\chi(q,\omega')]}{\omega' - \omega}. \tag{3}$$

$\chi(q,0)$, which is purely real, can be calculated by setting $\omega = 0$ in Eq. (3). The integration in $\omega' < 0$ was performed using the property that $\mathrm{Im}[\chi(q,\omega')]$ is an odd function. The integration of the K–K relation was performed up to 350 eV to ensure the causality. Thus the experimentally obtained $\chi(q,0)$ includes the contribution of the core electrons as well as that of the valence electrons.

Figure 3(a) shows the experimentally determined $\chi(q,0)$. For comparison with the experimental results, we calculated $\chi(q,0)$ of the electron gas model within the RPA. The calculated results were convolved with a Gaussian, representing the experimental resolution of 0.136 Å^{-1}. The absolute scales of the experimental results are comparable to that of the electron gas model, however, their scales change depending on the normalization method. Thus, we calculated the normalized density response function $\overline{\chi}(q,0) \equiv \chi(q,0)/\mathrm{Max}|\chi(q,0)|$ to compare the shape of the response function. Figure 3(b) shows $\overline{\chi}(q,0)$ for norm 1. The experimentally determined $\overline{\chi}(q,0)$ for the solid and liquid quantitatively reproduces the characteristics of the electron gas results. Figure 3(c) shows $\overline{\chi}(q,0)$ for norm 2, and its q dependence is similar to that for norm 1, however, $\overline{\chi}(q,0)$ of norm 2 shows a bent at $q > 2.8k_F$. This feature should be an artifact arising from the normalization, because in this q range a large part of the sum integral of norm 2 was evaluated from the extrapolated curve and the uncertainty due to the extrapolation is large, seen from the Fig. 1(d).

We calculated the derivative of $\overline{\chi}(q,0)$ to investigate the $2k_F$ singularity. Figure 4(a) shows $\overline{\chi}(q,0)$ for the solid and liquid. A noteworthy feature is that the experimentally determined $\Delta\overline{\chi}(q,0)/\Delta q$ exhibits a maximum near $2k_F$. The peak

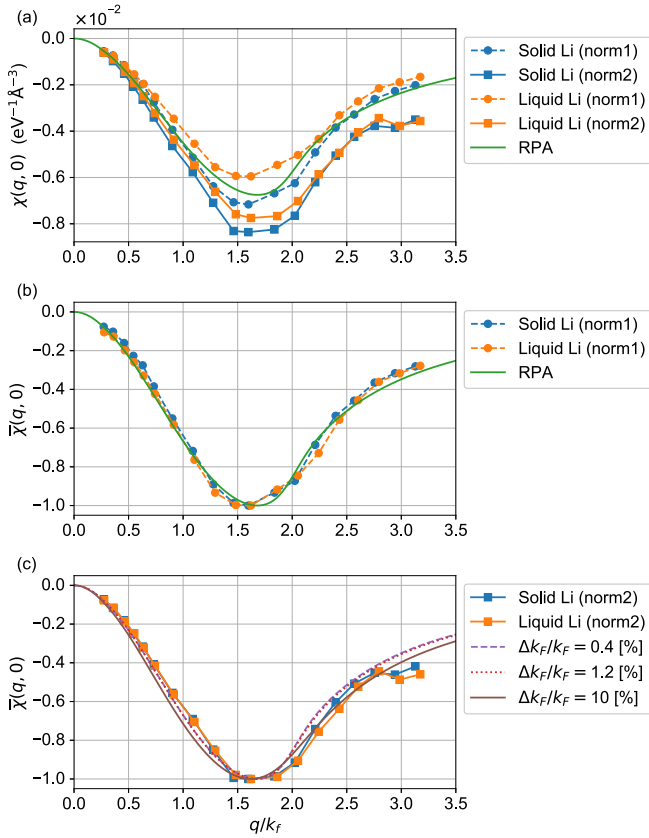

FIG. 3. (a) Experimentally obtained $\chi(q, 0)$ in solid Li and that of the electron gas model. The different normalization methods are indicated in the legend. The solid line is the calculated result for the electron gas model within the RPA. (b) The normalized density response function $\overline{\chi}(q, 0)$ for norm 1. (c) Corresponding results for norm 2 are compared with the calculated result including the effect of Fermi surface blurring. q is scaled by the Fermi wave vector with $k_F^{\mathrm{sol}} = 1.11$ Å^{-1} and $k_F^{\mathrm{liq}} = 1.09$ Å^{-1}.

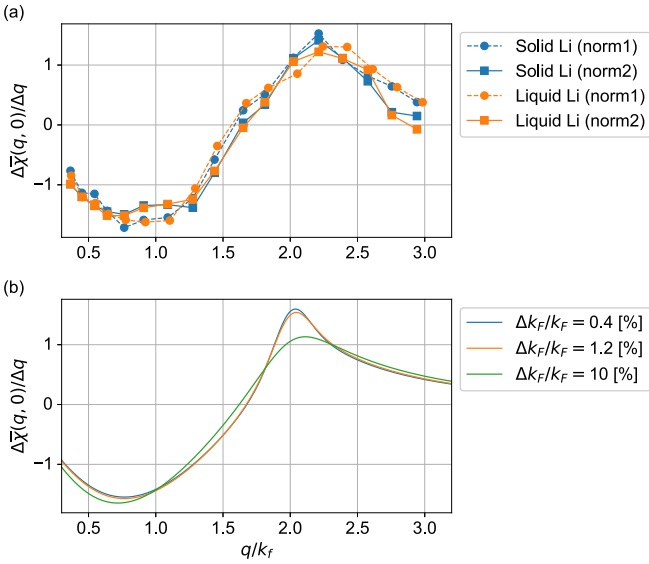

FIG. 4. (a) Derivative of $\overline{\chi}(q, 0)$ for solid and liquid Li. (b) Corresponding results including the effect of Fermi surface blurring.

TABLE I. Electrical resistivity, mean free path, and ratio $\Delta k_F/k_F$.

	$\rho(\Omega \cdot \mathrm{m})$	l (Å)	$\Delta k_F/k_F$ (%)
Solid Li	8.55×10^{-8} [37]	115.2	0.4
Liquid Li	26.33×10^{-8} [38]	38.5	1.2
Liquid Li		4.6	10 [39]

must reflect the logarithmic divergence of $\Delta\overline{\chi}(q, 0)/\Delta q$, as is predicted in the electron gas model. Moreover, the peak in the liquid is broader than in the solid. As previously mentioned, the shape of the IXS spectra in this q range actually changes upon melting, and this trend suggests that the effect of the $2k_F$ singularity in the liquid is weaker than in the solid.

To investigate the $2k_F$ singularity in the solid and liquid, we calculated $\overline{\chi}(q, 0)$ which includes the effect of Fermi surface blurring, using the dielectric function $\varepsilon(q, l)$ derived by Leavens *et al.* [29]. In $\varepsilon(q, l)$, the effect of Fermi surface blurring is expressed with the mean free path l. According to the Heisenberg uncertainty principle, the blurring of k_F can be roughly estimated to be $\Delta k_F \sim 1/(2l)$. In Table I, we list Δk_F and l, which are estimated from the electrical resistivity. However, the estimated $\Delta k_F/k_F$ of the liquid is much smaller than that calculated by the Green function method [39] (see Table I). In liquid metals, the electronic state is strongly influenced by the scattering effects of disordered ions, and it is necessary to fully take this into account for the estimation of Δk_F. The scattering effects of disordered ions are included in the self-energy calculated by Yan [39], and Δk_F estimated by the Green function method is more accurate than the estimation using the electrical resistivity. We also carried out the calculation by setting the parameter l such that Δk_F is equal to the value calculated by Yan [39]. The conditions for the calculation of $\varepsilon(q, l)$ are listed in Table I [40].

The results of $\overline{\chi}(q, 0)$ calculated from $\varepsilon(q, l)$ are shown in Fig. 3(c). In the solid, there is only a small difference between results calculated with and without Fermi surface blurring. In the liquid, the result calculated with $\Delta k_F/k_F = 10\%$ shows a broad peak compared to that compared with the result with $\Delta k_F/k_F = 1.2\%$. Figure 4(b) shows $\Delta\overline{\chi}(q, 0)/\Delta q$ which includes the effect of Fermi surface blurring. The peak near $q = 2k_F$ is broadened as $\Delta k_F/k_F$ increases, however, the calculated broadening of the peak is large compared with the experimentally obtained trend. Thus, the feature of the $2k_F$ singularity is less pronounced in the liquid because of the effect of disorder, however, this effect is smaller than theoretically expected.

C. Screening electron density

To investigate screening in real space, we have calculated the screening electron density $\Delta n(r)$ [13]:

$$\Delta n(r) = \frac{1}{2\pi^2}\int_0^\infty dq\left(\frac{q\sin qr}{r}\right)\chi(q, 0)\frac{4\pi e(-e)}{q^2}, \qquad (4)$$

where we assumed the external potential of a positive point charge. As the q range of the experimental results was limited, we extrapolated the data using the response function

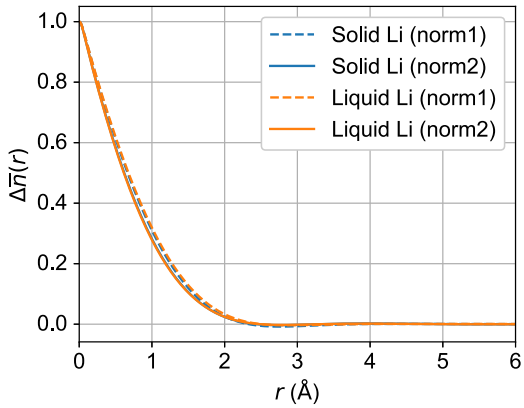

FIG. 5. Screening electron density of Li.

of the RPA. The extrapolated results well reproduce the q dependence of the experimental results (see the Supplemental Material [34]).

Figure 5 shows the normalized screening electron density $\Delta\overline{n}(r) \equiv \Delta n(r)/\mathrm{Max}|\Delta n(r)|$. The electrons aggregate to the positive charge at $r = 0$, and they form the screening in the range of about 2.2 Å. This value is estimated from the distance at which $\Delta\overline{n}(r)$ decays to 1% of $\Delta\overline{n}(0)$.

Figures 6(a)–6(c) show an enlargement of $\Delta\overline{n}(r)$ at large r. In addition to the screening near the positive charge, electron density oscillations over a long range are observed both in the solid and liquid. For $\Delta\overline{n}(r)$, the effect of a systematic error is large compared with the case of $\overline{\chi}(q, 0)$. The oscillations of the liquid for norm 1 is distorted in $r < 5$ Å. We estimated the wavelength of the oscillations from the maximum and minimum positions in $r > 5$ Å as:

$$\lambda = \frac{\sum_1^{N_1}\left(r_{i+1}^{\max} - r_i^{\max}\right) + \sum_1^{N_2}\left(r_{i+1}^{\min} - r_i^{\min}\right)}{N_1 + N_2}, \qquad (5)$$

where $r_i^{\max}$ and $r_i^{\min}$ are the maximum and minimum position, respectively. We calculated the wave vector from the wavelength of norm 1 and obtained $K_{\mathrm{norm1}}^{\mathrm{sol}} = (1.93 \pm 0.05)k_F^{\mathrm{sol}}$ and $K_{\mathrm{norm1}}^{\mathrm{liq}} = (2.18 \pm 0.19)k_F^{\mathrm{liq}}$. In the case of norm 2, the value is $K_{\mathrm{norm2}}^{\mathrm{sol}} = (2.07 \pm 0.27)k_F^{\mathrm{sol}}$ for the solid. For the liquid, it is difficult to determine the wave vector, because the amplitude of the oscillations in $6 < r < 8$ Å is too small to detect the maximum and minimum positions. Alternatively, we estimated the wave vector for the liquid by including the peaks in $r < 5$ and obtained $K_{\mathrm{norm2}}^{\mathrm{liq}} = (2.16 \pm 0.08)k_F^{\mathrm{liq}}$. The obtained wave vectors are in reasonable agreement with the wave vector of the Friedel oscillations. Furthermore, in $r > 7.5$ Å the Friedel oscillations in the liquid tend to be smaller than in the solid, for both cases of norm 1 and norm 2. This difference should reflect the sharpness of the Fermi surface, because it has been pointed out that the amplitude of the Friedel oscillations in the effective interionic potential becomes small if the Fermi surface is blurred [28,30]. We calculated $\Delta\overline{n}(r)$ including the effect of Fermi surface blurring, and the calculated results are shown in Fig. 6(d). The damping of the Friedel oscillations is enhanced with increasing $\Delta k_F/k_F$, and

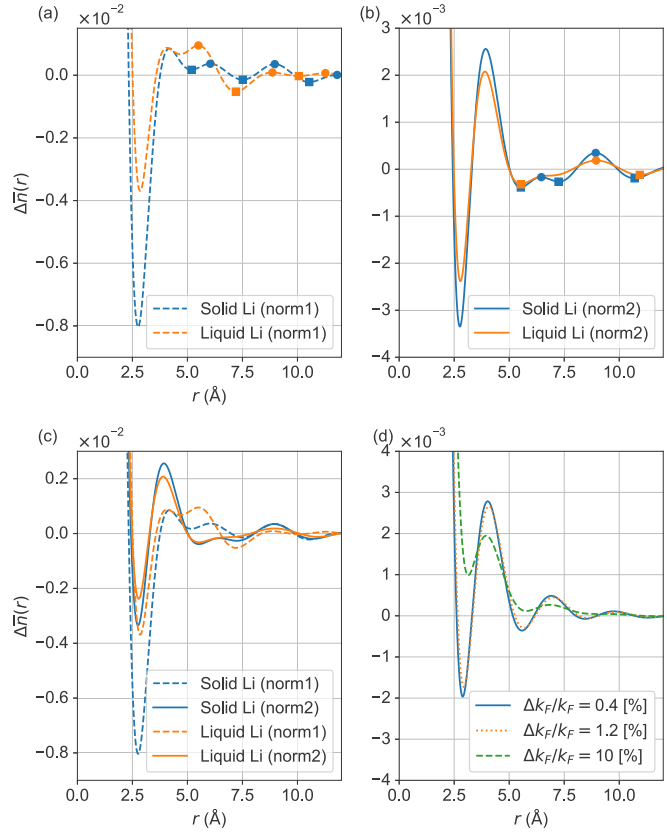

FIG. 6. (a) Enlargement of the long-range oscillations in $\Delta\overline{n}(r)$ calculated by the method of norm 1. The maximum and minimum positions of oscillations are indicated by circles and squares, respectively. (b) Corresponding results of norm 2. (c) Comparison of the results of norm 1 and norm 2. (d) Calculated $\Delta\overline{n}(r)$ including the effect of Fermi surface blurring.

the amplitude of the Friedel oscillations with $\Delta k_F/k_F = 10\%$ is especially small. These calculations qualitatively reproduce the trend of the experimental results on melting, which shows that the variation of the Friedel oscillations upon melting is caused by the Fermi surface blurring. It is noted that the blurring effect is more clearly observed in $\Delta\overline{n}(r)$ for norm 2 than $\Delta\overline{\chi}(q, 0)/\Delta q$. However, the observed change of $\Delta\overline{n}(r)$ is not as large as that of the Green function method, as in the case of $\overline{\chi}(q, 0)$. This indicates that the Friedel oscillations slightly weakened by the effect of disorder persist in the liquid state near the melting point.

We calculated the total induced charge to discuss the accuracy of the absolute scales of $\chi(q, 0)$, which is determined by the f-sum rule. The accuracy of the absolute scale can be checked by the condition that the integrated screening electron density for a positive charge is $-e$ [41], which means that screening is complete. We calculated the total induced charge as $Q = -e\int_0^\infty dr 4\pi r^2 \Delta n(r)$ and obtained $Q \approx -0.9e$ for both the solid and the liquid in the case of norm 1. In the case of norm 2, we obtained $Q \approx -1.2e$ for the solid and $Q \approx -1.1e$ for the liquid. These values are comparable to $-e$, however, they change depending on the normalization method. Thus, we discussed the normalized quantities, $\overline{\chi}(q, 0)$ and $\Delta\overline{n}(r)$.

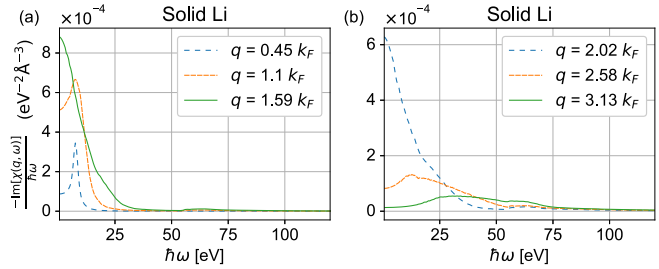

FIG. 7. (a) $\frac{-\mathrm{Im}[\chi(q,\omega)]}{\hbar\omega}$ of solid Li in the low q region and (b) high q region.

D. Effect of the core electrons on screening

Finally, we comment on the effect of the core electrons on $\overline{\chi}(q,0)$. In fact, $\overline{\chi}(q,0)$ is influenced by the contribution of the core electrons in $\mathrm{Im}[\chi(q,\omega)]$ through the K–K relation. Figure 7 shows the integrand of the K–K relation $(\mathrm{Im}[\chi(q,\omega)]/\omega)$. The core contribution, in $\hbar\omega > 55$ eV, increases with q, and this contribution is not negligible in $q > 2k_F$. To illustrate this effect, we calculated $\overline{\chi}(q,0)$ which only includes the contribution of the valence electrons. To remove the core contribution, we calculated $\overline{\chi}(q,0)$ by the K–K transformation of $\mathrm{Im}[\chi(q,\omega)]$ extrapolated by Mermin's function. Figure 8(a) shows the results of $\overline{\chi}(q,0)$ with and without the core contribution. The effect of the core contribution is smaller than expected from the IXS spectra in Fig. 2(a). This is because the core contribution, located in the high energy region, is weakened by a factor of $1/\omega$ in Eq. (3). In $q > 2k_F$, $\overline{\chi}(q,0)$ of the valence contribution takes larger values than that of norm 2, and the valence results show a better agreement with that of the electron gas model. Thus, the valence contribution is well described by the electron gas model, however, the core contribution is also important for describing the screening property in the high q region. In this study, the experimental results are compared with the electron gas model within the RPA, however, the comparison with a sophisticated theoretical calculation including the effect of the band structure and the core electrons will lead us to deduce information on the many-body effect on the screening.

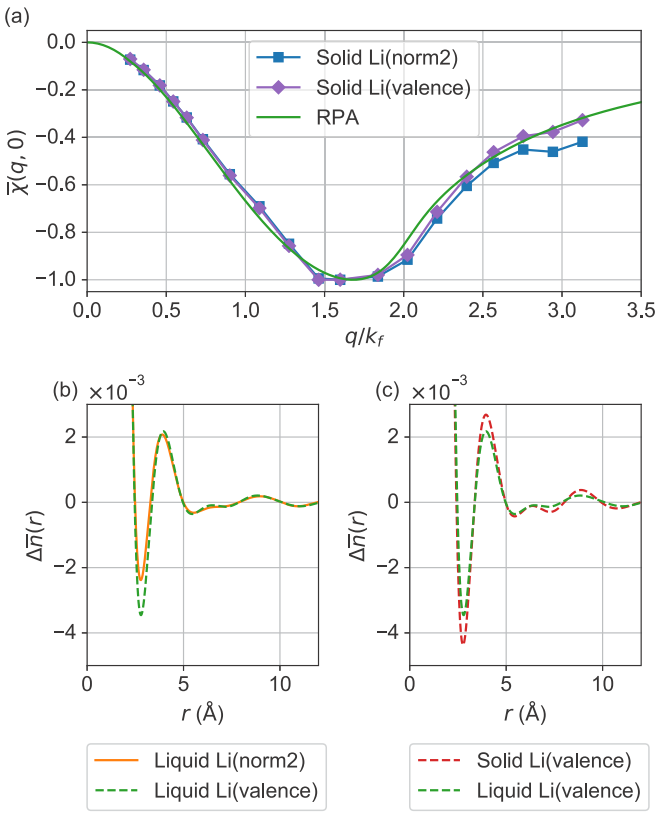

FIG. 8. (a) $\overline{\chi}(q,0)$ with and without the core contribution for solid Li. The calculation method for $\overline{\chi}(q,0)$ of the valence contribution is described in the text. (b) $\Delta\overline{n}(r)$ with and without the core contribution for the liquid. (c) $\Delta\overline{n}(r)$ for the valence contribution in the solid and liquid.

To investigate the effect of the core electrons on the screening electron density, we calculated $\Delta\overline{n}(r)$ from $\overline{\chi}(q,0)$ of the valence contribution. We compare $\Delta\overline{n}(r)$ for the liquid with and without the core contribution in Fig. 8(b). The amplitude of the Friedel oscillations for the valence contribution is larger than that for norm 2 in low r. This shows that the short-range oscillation becomes weak due to the effect of the core electrons, however, the long-range oscillations are not affected. Furthermore, we compared the $\Delta\overline{n}(r)$ of the solid and liquid for the valence contribution in Fig. 8(c). The amplitude for the liquid is smaller than that for the solid. This supports the interpretation that the Friedel oscillations become weak upon melting because of the Fermi surface blurring.

IV. CONCLUSION

We carried out IXS experiments on solid and liquid Li and experimentally determined the static density response function. The experimental $\chi(q,0)$ of a simple metal provides a testing ground for the theoretical description of screening and will contribute to improve the treatment of the many-body effects in the density functional theory. The experimentally determined $\chi(q,0)$ shows the $2k_F$ singularity predicted in the electron gas model. Moreover, we calculated the screening electron density and found that the amplitude of the Friedel oscillations in the liquid tend to be smaller than in the solid. This trend upon melting is explained by Fermi surface blurring due to the scattering effects of disordered ions.

ACKNOWLEDGMENTS

The authors would like to thank Y. Jeong, T. Sakurazawa, and A. Niozu for help with the measurements and also Prof. K. Nagaya for valuable discussions. This work was supported by JSPS KAKENHI (Research No. 18H01142) and the Toray Science Foundation. The synchrotron radiation experiments were performed at SPring-8 with the approval of the National Synchrotron Radiation Research Center, Taiwan (Proposals No. 2017-3-250-1, No. 2018-1-229-1, No. 2018-2-189-1, and No. 2018-3-180-1) and Japan Synchrotron Radiation Research Institute (Proposals No. 2017B4254, No. 2018A4253, No. 2018A4261, and No. 2018B4260).

[1] G. Giuliani and G. Vignale, *Quantum Theory of the Electron Liquid* (Cambridge University Press, New York, 2005).

[2] J. Lindhard, K. Dan. Vidensk. Selsk. Mat. Fys. Medd. **28**, 1 (1954).

[3] J. Friedel, Nuovo Cimento Suppl. **7**, 287 (1958).

[4] S. Ichimaru, Rev. Mod. Phys. **54**, 1017 (1982).

[5] S. Moroni, D. M. Ceperley, and G. Senatore, Phys. Rev. Lett. **75**, 689 (1995).

[6] M. F. Crommie, C. P. Lutz, and D. M. Elgler, Nature (London) **363**, 524 (1993).

[7] Y. Hasegawa and P. Avouris, Phys. Rev. Lett. **71**, 1071 (1993).

[8] M. Bouhassoune, B. Zimmermann, D. W. P. Mavropoulos, P. H. Dederichs, S. Blugel, and S. Lounis, Nat. Commun. **5**, 5558 (2014).

[9] Y. Hasegawa, M. Ono, Y. Nishigata, T. Nisho, and T. Eguchi, J. Phys.: Conf. Ser. **61**, 399 (2007).

[10] P. Mallet, I. Brihuega, V. Cherkez, J. M. Gmez-Rodrguez, and J.-Y. Veuillen, C. R. Phys. **17**, 294 (2016).

[11] K. W. Clark, X.-G. Zhang, G. Gu, J. Park, G. He, R. M. Feenstra, and A.-P. Li, Phys. Rev. X **4**, 011021 (2014).

[12] G. F. Giuliani and G. E. Simion, Solid State Commun. **127**, 789 (2003).

[13] G. E. Simion and G. F. Giuliani, Phys. Rev. B **72**, 045127 (2005).

[14] M. D. Johnson and N. H. March, Phys. Lett. **3**, 313 (1963).

[15] N. E. Cusack, *The Physics of Structurally Disordered Matter* (Hilger, Bristol, 1987).

[16] P. Abbamonte, K. D. Finkelstein, M. D. Collins, and S. M. Gruner, Phys. Rev. Lett. **92**, 237401 (2004).

[17] P. Abbamonte, G. Wong, D. Cahill, J. Reed, R. Coridan, N. Schmidt, G. Lai, Y. Joe, and D. Casa, Adv. Mater. **22**, 1141 (2010).

[18] W. Schülke, *Electron Dynamics by Inelastic X-ray Scattering* (Oxford University Press, Oxford, 2007).

[19] J. P. Reed, B. Uchoa, Y. I. Joe, Y. Gan, D. Casa, E. Fradkin, and P. Abbamonte, Science **330**, 805 (2010).

[20] P. Eisenberger, P. M. Platzman, and P. Schmidt, Phys. Rev. Lett. **34**, 18 (1975).

[21] G. D. Priftis, J. Boviatsis, and A. Vradis, Phys. Lett. A **68**, 482 (1978).

[22] H. Nagasawa, S. Mourikis, and W. Schülke, J. Phys. Soc. Jpn **58**, 710 (1989).

[23] W. Schülke, H. Nagasawa, and S. Mourikis, Phys. Rev. Lett. **52**, 2065 (1984).

[24] W. Schülke, H. Nagasawa, S. Mourikis, and P. Lanzki, Phys. Rev. B **33**, 6744 (1986).

[25] J. P. Hill, C. C. Kao, W. A. C. Caliebe, D. Gibbs, and J. B. Hastings, Phys. Rev. Lett. **77**, 3665 (1996).

[26] D. R. Gustafson, A. R. Mackintosh, and D. J. Zaffarano, Phys. Rev. **130**, 1455 (1963).

[27] A. T. Stewart, J. H. Kusmiss, and R. H. March, Phys. Rev. **132**, 495 (1963).

[28] T. Gaskell and N. H. March, Phys. Lett. **7**, 169 (1963).

[29] C. R. Leavens, A. H. Macdonald, R. Taylor, A. Ferraz, and N. H. March, Phys. Chem. Liq. **11**, 115 (1981).

[30] F. A. Oliveira and A. Ferraz, Solid State Commun. **52**, 963 (1984).

[31] N. Hiraoka, H. Fukui, H. Tanida, H. Toyokawa, Y. Q. Cai, and K. D. Tsuei, J. Synchrotron Rad. **20**, 266 (2013).

[32] The energy scan in $|\mathbf{q}| < 1.0$ Å^{-1} was carried out from -10 to 110 eV, because the plasmon excitation peaks appear in the low-energy region. Then, the tail of the spectra was extrapolated using the Lorentzian.

[33] N. D. Mermin, Phys. Rev. B **1**, 2362 (1970).

[34] See Supplemental Material at http://link.aps.org/supplemental/10.1103/PhysRevB.102.054208 for the details of this method and the variation of the IXS intensity.

[35] This extrapolation is based on the assumption that the excitation spectra can be described with the electron gas model. The extrapolation using the simulated results of the Li K edge should provide a more reliable result, and we hope to perform such simulation in future work.

[36] K. Sturm, Adv. Phys. **31**, 1 (1982).

[37] N. W. Ashcroft and N. D. Mermin, *Solid State Physics* (Thomson Learning, New York, 1976), p. 8.

[38] R. W. Ohse, *Handbook of Thermodynamic and Transport Properties of Alkali Metals* (Blackwells, Oxford, 1980), p. 730.

[39] X. Z. Yan, Phys. Rev. B **51**, 15823 (1995).

[40] Δk_F in the Green function method [39] is estimated using the following relation: $n(k_F + \Delta k_F)/n(k_F) = [1/(e+1)] \cdot [1/(1+1)]^{-1}$, where we assumed that the momentum distribution function is expressed as $n(k) = 1/\exp[\frac{E(k)-E(k_F)}{\Delta}]$ (Δ describes the blurring of the Fermi surface [28]).

[41] A. L. Fetter and J. D. Walecka, *Quantum Theory of Many-Particle Systems* (Dover, New York, 2003), p. 176.